

Hardwired-Neurons Language Processing Units as General-Purpose Cognitive Substrates

YANG LIU¹, YI CHEN^{1,2}, YONGWEI ZHAO¹, YIFAN HAO¹, ZIFU ZHENG¹, WEIHAO KONG¹, ZHANGMAI LI^{1,2}, DONGCHEN JIANG¹, RUIYANG XIA¹, ZHIHONG MA¹, ZISHENG LIU¹, ZHAOYONG WAN^{1,2}, YUNQI LU¹, XIMING LIU¹, HONGRUI GUO¹, ZHIHAO YANG³, ZHE WANG¹, TIANRUI MA¹, MO ZOU¹, RUI ZHANG¹, LING LI³, XING HU¹, ZIDONG DU¹, ZHIWEI XU¹, QI GUO¹, TIANSHI CHEN⁴, and YUNJI CHEN¹, ¹State Key Lab of Processors, Institute of Computing Technology, CAS, China, ²University of Science and Technology of China, China, ³Institute of Software, CAS, China, and ⁴Cambricon Technologies, China

The rapid advancement of Large Language Models (LLMs) has established language as a core general-purpose cognitive substrate, driving the demand for specialized Language Processing Units (LPUs) tailored for LLM inference. To overcome the growing energy consumption of LLM inference systems, this paper proposes a Hardwired-Neurons Language Processing Unit (HNLPU), which physically hardwires LLM weight parameters into the computational fabric, achieving several orders of magnitude computational efficiency improvement by extreme specialization. However, a significant challenge still lies in the scale of modern LLMs. An ideal estimation on hardwiring GPT-oss 120 B requires fabricating at least 6 billion dollars of photomask sets, rendering the straightforward solution economically impractical.

Addressing this challenge, we propose the novel *Metal-Embedding* methodology. Instead of embedding weights in a 2D grid of silicon device cells, Metal-Embedding embeds weight parameters into the 3D topology of metal wires. This brings two benefits: (1) a 15× increase in density, and (2) 60 out of 70 layers of photomasks are made homogeneous across chips, including all EUV photomasks. In total, Metal-Embedding reduced the photomask cost by 112×, bringing the Non-Recurring Engineering (NRE) cost of HNLPU into an economically viable range. Experimental results show that HNLPU achieved 249,960 tokens/s (5,555×/85× of GPU/WSE), 36 tokens/J (1,047×/283× of GPU/WSE), 13,232 mm² total die area (29% inscribed rectangular area in a 300 mm wafer), \$ 184 M estimated NRE at 5 nm technology. Analysis shows that HNLPU achieved 8.57× cost-effectiveness and 230× carbon footprint reduction compared to H100 clusters, under an annual weight updating assumption.

1 Introduction

The current trends in artificial intelligence development indicate that language capabilities serve as the core foundation for constructing advanced cognitive and learning systems. This is exemplified by the rapid advancement of Large Language Models (LLMs), which have achieved technological unification in Natural Language Processing (NLP) [7, 47, 52]. By demonstrating human-level performance across diverse downstream tasks, LLMs are expanding their application

Authors' Contact Information: Yang Liu¹; Yi Chen^{1,2}; Yongwei Zhao¹; Yifan Hao¹; Zifu Zheng¹; Weihao Kong¹; Zhangmai Li^{1,2}; Dongchen Jiang¹; Ruiyang Xia¹; Zhihong Ma¹; Zisheng Liu¹; Zhaoyong Wan^{1,2}; Yunqi Lu¹; Ximing Liu¹; Hongrui Guo¹; Zhihao Yang³; Zhe Wang¹; Tianrui Ma¹; Mo Zou¹; Rui Zhang¹; Ling Li³; Xing Hu¹; Zidong Du¹; Zhiwei Xu¹; Qi Guo¹; Tianshi Chen⁴; Yunji Chen¹, ¹State Key Lab of Processors, Institute of Computing Technology, CAS, China and ²University of Science and Technology of China, China and ³Institute of Software, CAS, China and ⁴Cambricon Technologies, China, {liuyang22z1,zhaoyongwei,haoyifan,zhengzifu24s,kongweihao21b,jiangdongchen23s,xiaruiyang,mazhihong24z,liuzisheng24s,luyunqi24s,liuximing22z,guohongrui21b,wangzhe24s,matianrui,zoumo,zhangrui,huxing,duzidong,zxu,guoqi,cyj}@ict.ac.cn,{chen_yi,lizhangmai,wanzhy}@mail.ustc.edu.cn,{yangzhihao2021,liling}@iscas.ac.cn,tchen@cambricon.com.

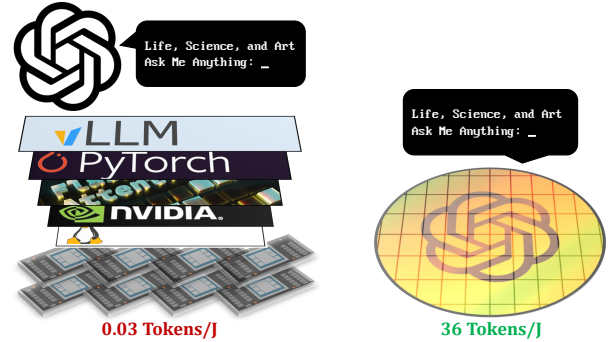


Fig. 1. Hardwired-Neurons LPU as a general-purpose processor. To the left: AI Infrastructures are originated in the rapidly evolving deep learning which appreciates universality over extreme efficiency. To the right: As LLM develops, the responsibilities of universality are shifting from HW/SW to LLMs. An extremely specialized Hardwired-Neurons LPU can also be helpful in general tasks.

scope while exhibiting a growing trend toward enhanced generality—enabling a single model to handle multiple tasks that previously required distinct systems.

Driven by the widespread adoption while heavy hardware overhead of LLMs, there has been a surge in demand for dedicated processors specifically designed for LLM inference, collectively known as Language Processing Units (LPUs). For instance, Groq LPU[4, 5] and Cerebras WSE[29, 31] pre-load model weights into on-chip SRAM, while Etched Sohu[3] hardens the transformer dataflow into its compute fabric. These LPUs leverage the advanced specialization targeting LLMs, achieving 4 ~ 20× energy efficiency compared to traditional CPUs, GPUs, and NPUs.

Although LPUs have brought a certain improvement in hardware efficiency, AI infra still suffers from tremendous energy cost. For example, AI datacenters are estimated to occupy 12% of the total electricity capacity in US before 2028, which is clearly unsustainable [39]. This is due to the fact that current LPUs and GPUs still see models as dynamically changing data, despite the fact that leading enterprises typically deploy only a single or a few proprietary LLM. The hundreds of billions of weight parameters are repeatedly fetched during each autoregressive decoding step, consuming the majority of system power.

To fundamentally solve the limitation, we argue to push the specialization of LPU to the extreme. By physically hardwiring

weight parameters into the LPU fabric, Hardwired-Neurons LPU (HNLPU) can achieve perfect architecture-model matching, zero parameter fetching overhead, and extreme computational efficiency from constants-arithmetic circuits. As one dominant pre-trained LLM can serve as a general-purpose cognitive substrate for a wide variety of tasks, the extreme specialization once considered too inflexible is transforming into a reasonable choice with huge potential benefits (Figure 1).

However, previous attempts on HNLPU would be stopped by the extraordinarily large scale of modern LLM. The most optimistic estimation on hardwiring GPT-oss 120 B [40] would require $176,000 \text{ mm}^2$ multiply-by-constant units (CMAC) array at 5 nm technology. Unlike previous wafer-scale practices stepping a repeated lithographic pattern on the wafer, here the patterns are heterogeneous everywhere, because embedded weight parameters are different everywhere. The photomask sets valued over *6 billion dollars*, rendering the straightforward implementation of HNLPU economically prohibitive.

Economically viable HNLPU must come after a weight-embedding methodology breakthrough. In this paper, we propose the Metal-Embedding (ME) methodology, achieving multiple order-of-magnitudes reduction on photomask counts required to implement HNLPU. Roughly speaking, instead of embedding weights in the 2D grid of cells (either MAC/CMAC/SRAM/ReRAM cells), ME embeds weights in the 3D topology of metal wires (Figure 2). The benefits of ME is two-fold. First, due to the inherently richer expression of 3D structure, ME reduced the area by an order-of-magnitude (-93.4%) compared with CMAC grid. Second, these metal wires can be placed at higher metal layers (M8+), to be cost-efficiently fabricated with trailing-edge optical lithography (193i). As a result, ME keeps photomask homogeneous (shared) across all chips for all layers in Front-End-of-Line (FEOL) and critical layers in Back-End-of-Line (BEOL), including all Extreme Ultraviolet (EUV) photomask in the process. This reduced the total cost on photomask by another order of magnitude: -86.5% for initial tapeout, -92.3% for parameter-only update re-spin.

We evaluate HNLPU at 5 nm technology based on post-layout characteristics, and compare with baselines (NVIDIA H100 GPU, Cerebras WSE-3) at the same technology node. Experimental results demonstrate that HNLPU achieved 249,960 tokens/s throughput ($5,555\times$ of H100, $85\times$ of WSE-3), 36 tokens/J energy efficiency ($1,047\times$ of H100, $283\times$ of WSE-3), at $13,232 \text{ mm}^2$ total die area divided into 16 chips. Estimated Non-Recurring Engineering cost (NRE) of HNLPU is \$ 184 M for the initial tapeout, \$ 44.3 M for a parameter-only update re-spin. Throughput per 3-Year Total Cost of Ownership (TCO) is $8.57\times/12.65\times$ of H100 clusters with/without annual parameter updates, and the total carbon footprint (tCO₂e) is reduced by $230\times/234\times$.

This paper makes the following contributions:

- We explored the concept and feasibility of HNLPU for the first time.
- We propose the Metal-Embedding methodology, reduced the photomask cost of HNLPU by two orders of magnitude.
- We detailed the architecture and dataflow of the first HNLPU design. It implemented a GPT-oss 120 B (FP4) in $13,232 \text{ mm}^2$

total die area, achieving unprecedented throughput and energy efficiency.

- We estimated the NRE, TCO, and tCO₂e of HNLPU to show its strong economical and environmental advantage for typical cloud serving scenarios.

2 Background and Motivation

2.1 Language as a cognitive substrate

Current AI development trends underscore language as the foundational substrate for constructing advanced cognitive capabilities. This centrality is supported by three key arguments. First, language is demonstrably critical to human intelligence. Neurocognitive research reveals strong correlations between linguistic competence and higher-order cognitive abilities, such as abstract reasoning [35]. These findings strongly suggest that language should similarly form the core of advanced artificial intelligence. Second, the sheer abundance of textual data vastly exceeds that available in other modalities. For instance, Common Crawl [12] has amassed an 8 PB text corpus from web pages, growing consistently by approximately 250 TB per month. This unparalleled scale of pre-training data is instrumental in enabling the zero-shot generalization abilities observed in Large Language Models (LLMs). Third, language constitutes the most natural and universal interface for human-AI collaboration. Robust language understanding and generation capabilities are indispensable for AI to integrate into human workflows and societal structures.

The rise of LLMs has further cemented language’s foundational status through technical unification. Historically, NLP was fragmented into specialized subfields (e.g., sentiment analysis, machine translation, named entity recognition), each requiring task-specific systems. Today, a single pre-trained LLM achieves state-of-the-art performance across common NLP tasks. This convergence stems from scaling model parameters and training data, enabling one general-purpose model to outperform prior specialized approaches. Consequently, LLMs now serve as universal engines for language-powered cognition, spanning reasoning, code generation, and multimodal interaction through linguistic interfaces.

This unification demonstrates that a single, highly capable LLM can function as a general-purpose cognitive substrate. While multiple implementations exist (e.g., GPT, Claude, Gemini, Qwen and DeepSeek), the focus of competition is shifting from capabilities to computational efficiency, a domain where model-architecture co-design becomes decisive. The demonstrated generality of modern LLMs makes architectural specialization strategically viable. For instance, models like GPT-oss 120 B which achieves state-of-the-art performance, exemplify how a singular, optimally scaled Transformer architecture can serve as a universal language engine. By fixing such a model as a standardized substrate, unprecedented hardware optimizations become feasible, while maintaining full generality through the model’s inherent language-based cognitive flexibility.

2.2 Specialized Language Processing Units

The emergence of LLM as universal cognitive engines has intensified demand for dedicated inference hardware. We define processors explicitly optimized for language models as Language Processing Units

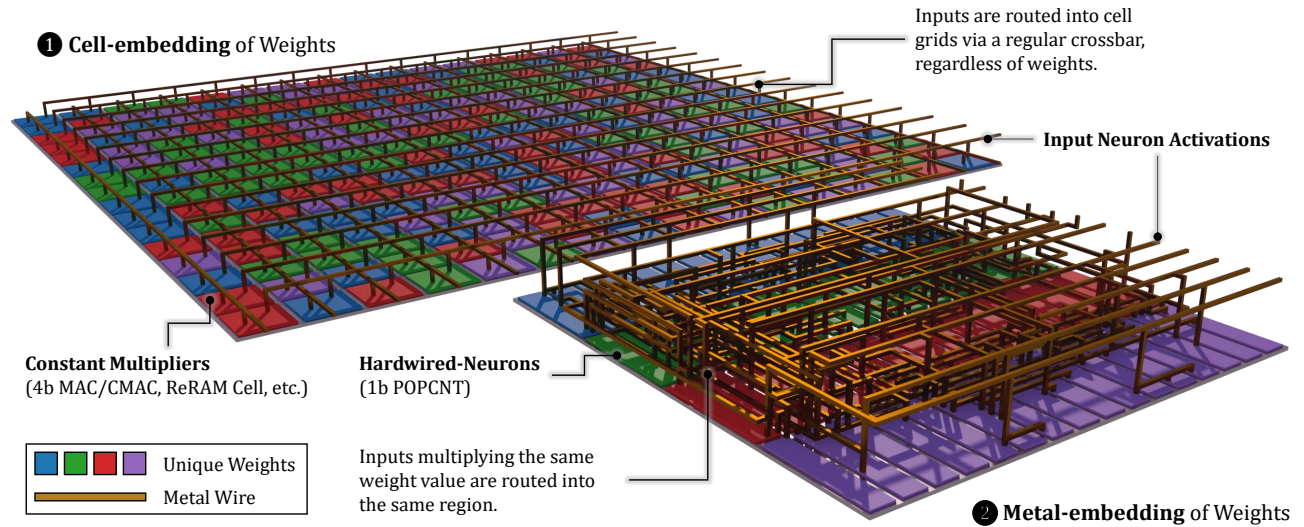


Fig. 2. Conceptual schematic of **Metal-embedding**. ❶ Conventional design embeds weights with 2D grid of cells. Metal layers are only for physical design (P&R). ❷ Metal-embedding dramatically increases the density by leveraging the 3D topology structure of metal wires, emulating the axon-dendrite in brains.

(LPUs), a complementary paradigm following CPUs/GPUs/NPUs. However, currently LPUs are predominantly repurposed from general-purpose processors. For example, the most widely-deployed NVIDIA Hopper architecture incorporates dedicated Transformer Engines, but still retains the architectural lineage of its Tensor Core GPUs originated before LLMs. These repurposed processors suffer from efficiency limitations intrinsic to their origin in more general applications, known as "Turing Tariffs" [25].

The major efficiency limitation in current architectures is two-fold. First, the architecture-model mismatch fails to accommodate divergent computational demands across inference phases (e.g., compute-bound prefill vs. memory-bound decoding), forcing industrial compromises like prefill/decode and attention/feed-forward decoupling that deploy heterogeneous hardware subsystems specifically [6, 48]. Second, repurposed processors dynamically load models as ever-changing data, despite the fact that enterprises typically deploy only a single or a few proprietary LLM. The >100 B model parameters are repeatedly fetched during each autoregressive decoding step, dominating the whole system power.

Emerging architectures like Cerebras Wafer-Scale Engine (WSE) and Groq LPU attempt to circumvent these bottlenecks through deterministic scheduling and massive on-chip SRAM integration, reportedly achieved up to $20\times$ energy efficiency gain over GPUs [5, 31]. These practices demonstrated the great benefits and viability of pushing the specialization of LPU hardware. However, Turing Tariffs still exist in these architectures. Only on one hand, parameter fetching still dominates the power consumption as the SRAM access cost is typically several times higher than computation [45].

To fundamentally address these limitations, we propose to push the specialization of LPU to an architectural extreme: permanent weight hardwiring within LPU chips. By physically embedding model parameters into the fabric of computing units, $\sim 1000\times$ efficiency gain could be obtained from perfect architectural matching,

zero parameter fetching overhead, and constant arithmetic. Such model-specialized architecture aligns with the industrial consolidation trend, where enterprises increasingly standardize on one dominant LLM architecture, transforming what was once considered an inflexibility into a fairly reasonable choice with huge potential benefits.

2.3 Hardwiring a Language Processing Unit

A glaring challenge has thwarted all ambitious attempts to hardwire the LPUs: *LLMs are too large for the current lithographic technology*. For example, the typical transistor density of high-density 5 nm technology is around 138 MTr/mm^2 . FP4 Constant MAC (CMAC) requires 200+ transistors. This translates GPT-oss 120 B into an ideal area estimation of $176,000 \text{ mm}^2$, four maximal inscribed rectangles in 300 mm wafer. Due to reticle size limits, this hardwired LPU has to split into 200+ sets of photomask. Unlike prior wafer-scale practices, these masks are heterogeneous. This incurs 6 billion dollars non-recurring engineering (NRE) costs on photomask making, rendering a straightforward hardwiring LPU economically prohibitive.

Compounding this economic infeasibility is the fast LLM development cycles. The absurdly high NRE is even worse when considering the annual parameter updates and 3-year typical lifespan of production LLMs (e.g., GPT-4). This multiple-orders-of-magnitude cost gap is unlikely to be bridged solely through model compression. Please note that the GPT-oss is already FP4 by default. The model size has a concrete lower bound implied by the Kolmogorov complexity of human knowledge representation.

To realize the concept of hardwired LPUs, there must be fundamental breakthroughs in the on-die weight embedding methodologies. By co-optimizing with lithography technology factors, we can achieve multiple orders-of-magnitudes reduction in photomask count, eventually clear the path to the economically viable hardwired LPUs.

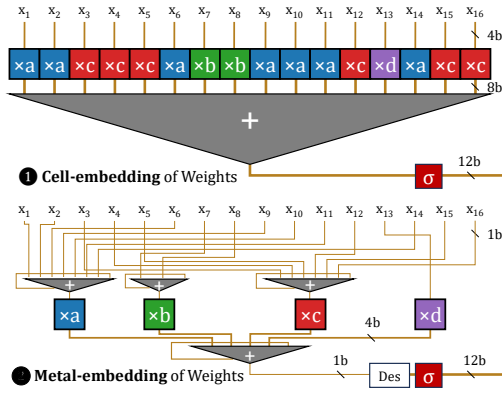


Fig. 3. Hardwired-Neuron architecture. ❶ A conventional cell-embedding neuron contains 2,880 4b multipliers (16 shown) followed by an $8b \times 2,880$ adder tree, where 2,880 is the hidden size in GPT-oss 120 B; ❷ With ME, Hardwired Neurons accept 1b serialized inputs (LSB-first), (1) route the inputs multiplying the same weight value to the same region, (2) perform counting (POPCNT) on these input signals, (3) perform actual multiplication with 16 multipliers (4 shown), (4) sum the results with a $4b \times 16$ adder tree. Note how ❷ is significantly smaller in area than ❶ by reducing the number of multipliers and the strength of adders.

3 Design Principles

Currently, almost all AI chips are designed as regular grid structures (Figure 2 ❶). Inputs, weights, and outputs are transmitted into/out-of the grid by a regular crossbar of metal wires. By fixing the weights, multipliers could be optimized as multiply-by-constant which is several times simpler in Boolean complexity. For example, FP4 multiply-by-constant is 42.5 Tr on average, $\sim 6\times$ smaller than FP4 multiplier. However, this density level is still far behind the requirement of HNLPU.

In current methodologies, metal layers are only considered during place-and-route (P&R), and the topology of metal wires do not express any specific information. We see this as a waste of resources. The key insight here is that, as the topology of metal wires are three-dimensional, they potentially could embed information in a much higher density than silicon devices. As silicon devices are the area-limiting factors in the design, routing signals through complex metal wires is almost free in both area and energy, compared with logic implemented in standard cells. Please recall that biological neurons in our brains have complex topology of axon-dendrite interconnections in the first place, only then come synaptic weights.

Metal-Embedding Hardwired-Neurons. We conceptualize Metal-Embedding (ME) in Figure 2 ❷. Instead of embedding weights with 2D grid of cells (silicon devices), we choose to embed weights in 3D topology of metal wires. The die is split into Hardwired-Neurons (HNs, each HN is drawn as a \curvearrowright row in the schematic), each HN corresponds to an output neuron activation in the model. Each HN is divided into several regions (different coloring in the schematic), where each region represents a unique weight value. For 4b precision models, there are $2^4 = 16$ unique values (4 shown in the schematic). To multiply with a weight, the input neuron activation signal is routed into the corresponding region via metal wires. Specifically,

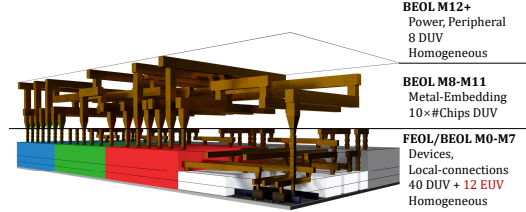


Fig. 4. Co-optimizing Metal-Embedding with technology. The embedding metal wires are routed at higher level (M8-M11), leaving other layers (devices, cell-level/module-level interconnections, power and peripherals) homogeneous in structures. As a result, all HNLPU chips could share the same set of photomask at layers other than M8-M11, including all critical layers which require expensive EUV photomask.

each input signal is multiplying with 2,880 weights (16 shown in the schematic) in GPT-oss 120 B: The model weights are solely embedded within the metal interconnection, expressed by connecting each input signal with corresponding regions.

Then HN carries the multiplying per region, as shown in Figure 3 ❷. As all input signals x_1, x_2, \dots, x_n in the same region are multiplying with the same constant weight value a , instead of performing $ax_1 + ax_2 + \dots + ax_n$, HN performs $a(x_1 + x_2 + \dots + x_n)$ by applying the distributive law. Furthermore, if input signals x_1, x_2, \dots, x_n are in binary format, it could be serialized from the least-significant bit (LSB) to the most-significant bit (MSB) to further simplify the circuit. After serialization, the arithmetic per region is reduced to a population count (POPCNT) followed by a constant-multiplication. The partial results from regions are then summed with a now much smaller adder tree.

Specifically, a conventional cell-embedding neuron (Figure 3 ❶) requires 2,880 $4b \times 4b$ multiply-by-constant, followed by an $8b \times 2,880$ adder tree. A ME HN (Figure 3 ❷) reduced the arithmetic strength to $(2,880 \text{ in total}) \times 1b$ POPCNT, followed by 16 $4b \times 1b$ multiply-by-constant and a $4b \times 16$ adder tree. By removing the weight embedding from area-limiting silicon layers, ME HN reduced the area by an order-of-magnitude, which we will demonstrate with post-layout evaluations.

Co-optimizing with lithography technology. Another opportunity brought by ME is to co-optimize with lithography to save photomask. Photomask sets account for the dominant part of NRE for HNLPU. Previous chiplet or wafer-scale designs always share one or few sets of photomask across chiplets/wafer-tiles, since they are designed as homogeneous structures. However, each chip in HNLPU is embedding different part of the model weights, they are heterogeneous in nature. Even with significantly reduced area of ME HN, HNLPU still requires 16 full mask sets, each valued around \$ 30 M at 5 nm technology. The total NRE still offset most economical interests considering the typical lifespan of LLMs.

Currently, mainstream 5 nm technology is mixing Extreme Ultraviolet Lithography (EUV) with Deep Ultraviolet Lithography (DUV) in the process. DUV (193i) can achieve 40~45 nm half-pitch with single exposure, smaller dimensions require multiple patterning techniques. EUV has finer resolution (13 nm half-pitch) due to significantly reduced wavelength. When applied on critical layers (e.g.

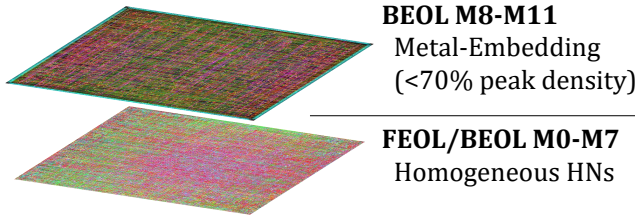


Fig. 5. Layout of a selected group of HNs.

fin cuts, contacts, lower metals M0-M3), single exposure of EUV can effectively replace 3~4 masks of multiple patterning if using DUV otherwise. However, EUV light beams with extremely short wavelength can no longer passthrough the transparent optical photomask used in DUV. Reflective photomask made of novel materials is required, which is around 5~8 \times more expensive than transparent optical mask.

If critical layers (silicon and lower metals) are made homogeneous, their photomasks could be reused across chips, then the total NRE will be significantly reduced. Therefore, we propose to place the ME only in higher metal layers (M8+) to enable cost-efficient fabrication with DUV, as shown in Figure 4.

This requires a moderate change in the IC design flow. Similar to the *sea-of-gates* architecture [14] emerged in 1990s which prefabricate gates on wafers, we prefabricate HNs, resulting in a *sea-of-neurons* architecture. First, we complete the physical design of a group of homogeneous HNs as a repeating pattern. As homogeneous HN design can no longer assume the number of input signals in each region, the POPCNT is divided into smaller slices and reconfigured with ME, instead of sizing on demand. Specifically, for GPT-oss 120 B there are 106 32b POPCNT slices in each HN, sufficiently reconfigurable for all assignments of the 2,880 inputs. The ports of POPCNT are routed up to M7, left for ME (VIA7) to connect. Then, the layout of HN is copied to fill the major part of die area, equipped with all SoC peripherals, power grid, and clock tree. Finally, each chip is individually wired at M8+ to embed their part of model weights. Figure 5 shows the layout of a randomly selected group of HNs, divided into homogeneous structures (M7-) and ME at the top (M8-M11). ME yielded a congestion-free layout (peak density <70%, zero overflow) and achieved timing closure at 1 GHz. The final design passed all DRC and LVS sign-off checks.

As a result, all HNLPU chips could share the same set of photomask at all layers other than M8-M11. At the scale of 16 chips, the estimated cost on photomask reduced from \$ 480 M to \$ 65 M. Furthermore, a parameter-only update can share the photomask set or build upon the prefabricated wafers with sea-of-neurons, thus the cost is estimated at \$ 37 M.

4 Architecture

In this section, we introduce the architecture of HNLPU in a top-down manner, as shown in figure 6, including system integration and single chip architecture.

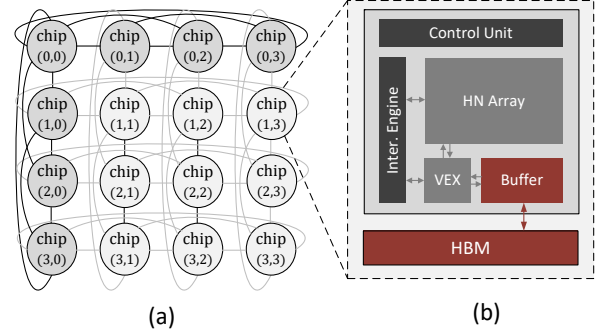


Fig. 6. The overall architecture of HNLPU system. (a) System-level architecture of HNLPU, featuring a logical 4 \times 4 row-column fully-connected fabric to interconnect its 16 modules. (b) Architecture of a single compute module, comprising the core die and HBM.

4.1 System Integration

Interconnection topology. The HNLPU system architecture is built upon a 16-module row-column fully-connected fabric. As conceptually illustrated by the logical topology in Figure 6(a), this fabric establishes direct, point-to-point links from each module to all other modules within its row and, simultaneously, to all other modules within its column. This design creates a router-less low-latency network for efficient collective communication patterns (e.g., All-Reduce). Each compute module is a self-contained unit, equipped with a dedicated HBM for storing the KV Cache and the embedding tables.

Multi-chip group mapping. HNLPU evenly distributes its constituent chips into multiple row- and column- groups, with each row and column containing 4 chips. This grouping strategy enables a parallel mapping of the self-attention and feed-forward network—the most computationally intensive parts of a Transformer block. Specifically,

- (1) For the GQA projection, the projections for all query, key, and value heads are uniformly mapped to their respective column groups.
- (2) For attention score, query-head is all-reduced within the same column groups, while key- and value- heads are reduced to the chip- $(\ell \bmod 4)$, where ℓ denotes the sequence length).
- (3) For the feed-forward network with MoE, all experts are uniformly distributed to all chips, and the input vector broadcasts to all chips. Specifically, each chip is responsible for 8 experts.

this group mapping strategy of HNLPU offers two key advantages. First, by distributing the GQA computation uniformly, the workload is balanced across all chips. This alleviates pressure on key computational resources (e.g., VEX units) and reduces the storage and bandwidth demands on the SRAM and HBM. Second, the independence of the MoE experts enables fully parallel FFN computation, eliminating the need for data exchange during the projection steps. The detailed execution process and dataflow are further elaborated in Section 5.

Physical System Integration. The physical implementation of HNLPU is based on established, industry-validated High-Performance Computing (HPC) integration practices.

Packaging: Each compute module utilizes 2.5D packaging to integrate a large monolithic die with its dedicated HBM stacks (conceptual topology is similar to the NVIDIA Blackwell platform).

Inter-Chip Communication: Direct point-to-point interconnects are established via the CXL 3.0 protocol (on PCIe PHY). This open standard offers low latency (<100 ns) and high bandwidth (128 GB/s per $\times 16$ link), with performance approaching proprietary solutions (e.g., NVIDIA NVLink).

Manufacturing Yield: The modular design enables a "Known-Good-Module" strategy. Each packaged module is tested independently, thus decoupling the final system's assembly yield from the challenging manufacturing yield of the large monolithic dies.

Thermal Management: For high thermal density, a Direct-to-Chip Liquid Cooling (DLC) solution is employed by mounting a cold plate on each module—an approach validated in compute platforms such as the NVIDIA DGX H100.

4.2 Single Chip Architecture

As shown in Figure 6(b), each chip in HNLPU is composed of five primary modules. The HN Array and VEX Unit are responsible for the LLM computation, including operations on hardwired weights, attention mechanisms, and nonlinear activation functions. The Attention Buffer serves as the on-chip KV Cache. Finally, the Control Unit manages on-chip scheduling and inter-layer pipelining for multi-batch scenarios, while the Interconnect Engine facilitates inter-chip communication.

The HN Array is a dedicated unit for performing computations that involve the *fixed and pre-trained* weights. As shown in Figure 3, we use metal embedding strategy to hardwire all the weights in the LLM onto the chip. Although the HN Array has a large area, its power consumption is remarkably low. This efficiency stems from the high sparsity of circuit activity: only 4 out of 128 experts are active at any given time in the target MoE architecture. For weight matrices (e.g., W_{qkv}) that are partitioned across multiple chips, each HN Array computes a partial sum. This result is then forwarded to the Interconnect Engine for aggregation with corresponding partial sums from other chips.

The Vector Execution Unit (VEX) is responsible for executing vector and matrix operations, including calculating attention scores, applying nonlinear functions (e.g., RMSNorm, SwiGLU, softmax), performing residual additions, and handling output sampling. 1) VEX adopts the FlashAttention computation flow to calculate attention scores. The hardware implementation consists of GEMV units and nonlinear operators. It fetches queries from the Interconnect Engine and reads keys/value (K/V) pairs from the on-chip Buffer. For each chip, the VEX unit is designed to process 32 cached KV-heads per cycle without stalling. 2) VEX also integrates dedicated nonlinear modules for the efficient computation of RMSNorm, SwiGLU, and softmax operations. Additionally, it includes a vector-aligned adder for residual connections and a specialized unit to perform multinomial sampling.

Attention Buffer. On each chip, the Attention Buffer provides

320 MB storage with a high throughput of 64 TB/s. It primarily functions as a KV Cache for the chip's assigned attention groups. It offloads excess KV entries to HBM only when the on-chip capacity is exceeded. This buffer also stores activation vectors for residual connections in the FFN blocks.

Interconnect Engine and Control Unit. The Interconnect Engine and Control Unit on each chip jointly manage all inter-chip communication and data collectives. The communication topology is organized into row-wise and column-wise groups, each with specific supported operations: 1) For row-wise communication, the system supports a *Broadcast* to distribute data (e.g., the activation vector) to all chips within the same row, and a corresponding *Reduce* operation to aggregate the partial sums computed by each chip in that row. 2) For column-wise communication, the system distributes inputs to chips within a column using either a *Scatter* operation, which provides each chip with a distinct portion of a vector, or a *Broadcast* operation, which provides all chips with the identical vector. To collect the results, the system supports both *Reduce* for aggregating partial sums and *Gather* for concatenating output vectors.

5 Execution Dataflow

In this section, we introduce the multi-chip interconnect dataflow of HNLPU, covering the model-to-chip mapping and the computing process of a Transformer block. In Section 5.1, we provide an overview of the HNLPU dataflow. Section 5.2 describes the computation of Group-Query Attention. In Section 5.3, we present the data flow for the MoE computation. Section 5.4 details our pipelining strategy and batching inference scheduling.

5.1 Dataflow Overview

Figure 7 illustrates the dataflow of HNLPU. Our design is driven by the primary goals of distributing computational, KV cache memory access, and thermal loads, while minimizing inter-chip data communication.

Processing begins with fetching a token vector of shape (1, 2880) from the High-Bandwidth Memory (HBM) based on the received token index. This vector then traverses through 36 transformer blocks, where self-attention and feed-forward network (FFN) computations are performed layer by layer. For the multi-head attention module, we employ a hybrid weight distribution strategy: the W_{qkv} weight matrix is partitioned column-wise across different chip column groups, while the W_o weight matrix is partitioned row-wise across the same set of chips. This design allows for parallel, independent computation across different chip columns for the W_{qkv} operations and across different chip rows for the subsequent W_o computations, thereby minimizing inter-chip data transfer.

The FFN implementation, which uses a Mixture-of-Experts (MoE) architecture, assigns eight experts to each chip, allowing for entirely independent computation with no inter-chip communication. A key exception to our partitioning strategy is the router's weight matrix, W_{rout} , which is replicated across all chips. This deliberate design trade-off introduces a negligible area overhead—as the router's weights constitute only about 0.01% of the total model weights—but eliminates the communication latency. Once all transformer blocks

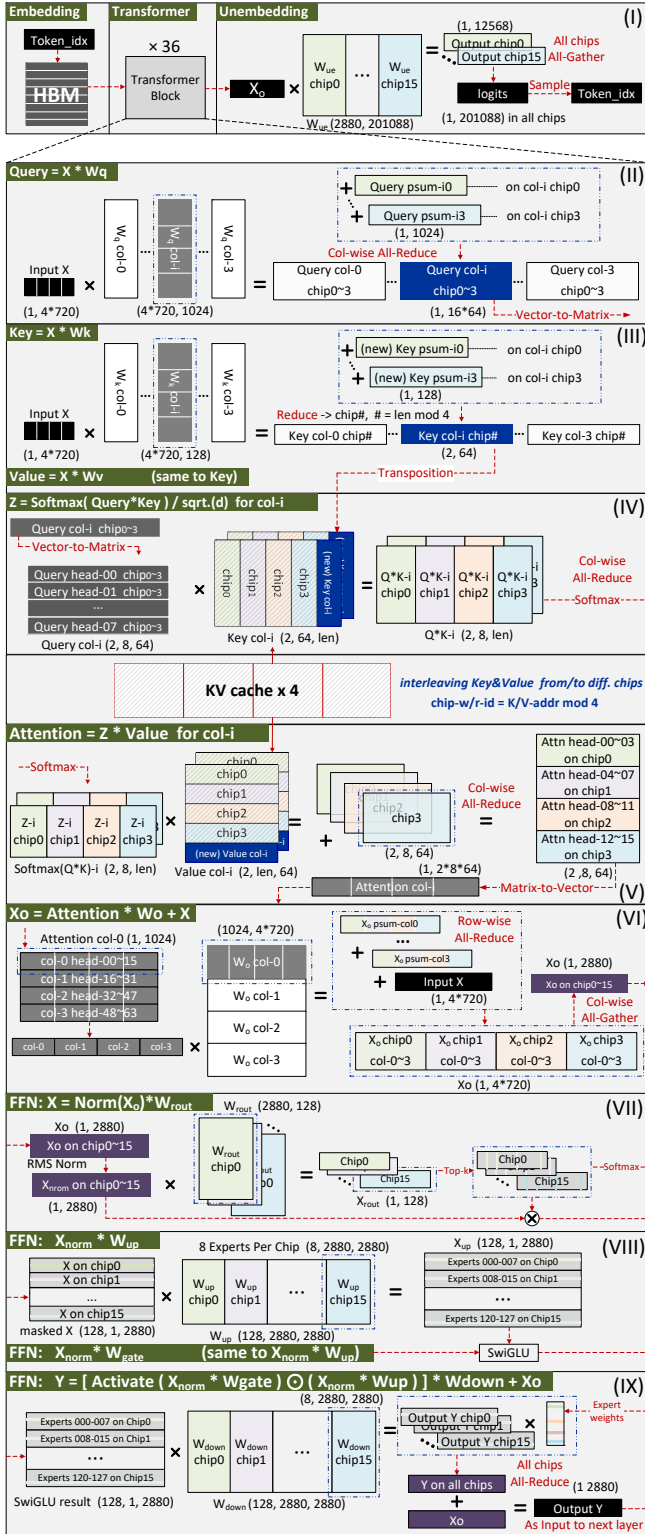


Fig. 7. Dataflow and mapping of HNLPU. (I) Overview of dataflow. (II) Query projection. (III) Key and Value projection. (IV&V) Attention score. (VI) Post-attention residual addition. (VII) Router in MoE. (VIII) Up- and Gate-projection. (IX) Down-projection and residual addition.

have been processed, the final output vector is passed through the unembedding layer, and a new token index is calculated through a sampling operation.

5.2 Grouped-Query Attention

Figure 7.(II) illustrates the computation dataflow of the 64 query heads projection. The token activation X that in the chip array has shape $(1, 2880)$. The activation X in all chips is split into four equal slices of $(1, 720)$ and each chip takes one of slices to calculate the partial sum of the query tensor. Each chip contains a private, hard-wired slice of W_q with shape $(720, 1024)$ inside the HN array. Therefore the product is generated locally and without any weight fetch. The four partial products are summed by a column-internal reduce operation, yielding 16-heads query vector $(1, 1024)$. The 16 query heads are then reshaped into $(2, 8, 64)$, representing that in Grouped-Query Attention, every 8 query heads correspond to a single KV head.

Figure 7.(III) follows a similar spatial pattern for the key path. Each chip multiplies its $(1, 720)$ input slice with its hard-wired W_k slice $(720, 128)$ and emits a partial key vector $(1, 128)$. After the column-internal reduction and reshape, the new key head of $(2, 64)$ is hold in chip# $(\# = \ell \bmod 4)$, where ℓ is the token's position in the sequence). At this point the data layout is intentionally asymmetric: the query vector is fully replicated across columns, whereas each key vector is unique per chip in the sequence dimension, a choice that minimises the traffic of the forthcoming dot-product. The data flow of $X * W_v$ is the same as that of W_k .

Figure 7.(IV) shows the computation of attention weight Z in column- i chips. Every chip already has the complete duplicate of the column- i Q heads $(2, 8, 64)$. The key tensor is partitioned horizontally, each chip keeps cached K with shape $(2, 64, \ell/4)$ in its local KV-cache (ℓ is the current context length). The VEX unit multiplies the Q head $(2, 8, 64)$ with K $(2, 64, \ell/4)$ and produces the local attention weight Z $(2, 8, \ell/4)$. Because each chip sees only $\ell/4$ tokens, a column-wise all-reduce needed to perform, after which every chip completes the normalisation of its local fragment.

Figure 7.(V) completes the attention score. V is tiled exactly like K ; each chip reads a V slice $(2, \ell/4, 64)$ from its KV-cache. The VEX unit multiplies the V $(2, 8, \ell/4)$ with the local attention weight Z $(2, 8, \ell/4)$, and emits the partial- O tensors $(2, 8, 64)$. A column-wise all-reduce needs to perform to add the four partial- O tensors. After that, all chips in column- i contain the 16 heads of the attention score O with the shape $(2, 8, 64)$. Then, the matrix is flattened to the shape $(1, 1024)$ for the multiplication with W_o .

Figure 7.(VI) depicts the output projection and first residual path. After the attention score computation, each of the four chips in a same column now holds the same, flattened attention score for 16 heads. The W_o matrix is partitioned row-wise across the column group chips, with each column assigned a weight shape of $(1024, 2880)$ and each individual chip's HN array receiving a $(1024, 720)$. Each chip generates a partial- O of shape $(1, 720)$. These partial- O s are combined via one row-wise all-reduce and one column-wise all-gather to yield the final X_o of shape $(1, 2880)$ in all chips.

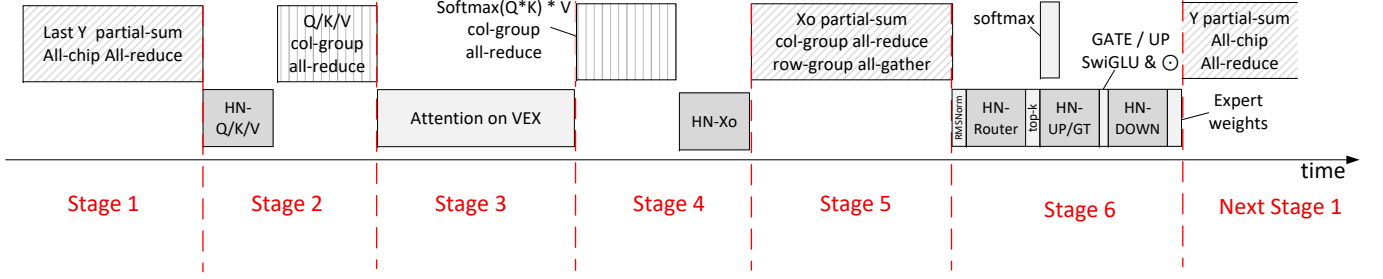


Fig. 8. A six-stage pipeline partitioning diagram for HNLPU dataflow.

5.3 Feed-Forward Network with MoE

Figure 7.(VII) shows the experts router stage. After the Group Query Attention computation, all chips in the HNLPU contain the complete $(1, 2880)$ X_o vector. These values are passed through RMSNorm before entering the routing layer. As W_{rout} only accounts for only about 0.01% of the total weights, we replicated a copy of the router weights on all 16 chips to avoid inter-chip data exchange. After the computation of $X_{\text{norm}} \cdot W_{\text{rout}}$, each chip obtains complete X_{rout} . Next, top-k and softmax operation are performed. The top-k result is used to generate a masked input tensor, X , with a shape of $(128, 1, 2880)$. In this tensor, the values for the top-k experts are set to those of X_{norm} , while all others are set to zero. Additionally, the top-k results are normalized with a softmax to obtain the expert weights.

Figure 7.(VIII) shows the up- and gate-projection stage. Following the top-k masking, each chip processes its masked X_{mask} tensor, which consists of 8 vectors, each of shape $(1, 2880)$. For 128 X_{mask} $(1, 2880)$ in all chips, only k of which are non-zero. The weight of W_{up} is sliced into 16 tiles, with the shape of $(8, 2880, 2880)$ for each chip. Then, the local 8 vectors of X_{mask} are multiplied with the sliced weight W_{up} of eight experts. The 16 chips produce a total X_{up} tensor of shape $(128, 1, 2880)$. Because each chip stores the complete weight matrices for all experts, this step requires no inter-chip data communication. The gate projection follows the same partitioning: X_{mask} is multiplied by the corresponding W_{gate} slice, yielding a X_G , $(128, 1, 2880)$ in total and $(8, 1, 2880)$ for each chip. Applying the SwiGLU activation to X_G and X_{up} , and taking the element-wise product, we get the output X_t for the subsequent down-projection.

Figure 7.IX shows the down-projection and second residual path. Still, X_t in each chip with the shape of $(8, 1, 2880)$ multiplies its down weight slice W_{down} , $(8, 2880, 2880)$, to produce a partial X_{down} , $(8, 1, 2880)$. Next, the expert weights, which were obtained from the previous stage (VII), are multiplied with the corresponding expert outputs to get the weighted output for each expert. Subsequently, an all-chip all-reduce operation is performed to sum the partial results. The shape of X_{down} in all chips is from $(128, 1, 2880)$ to $(1, 2880)$. The summed X_{down} is then added to X_o to yield the final layer output Y $(1, 2880)$.

5.4 Pipeline and Scheduling

HNLPU employs a nested pipelining strategy to maximize throughput, consisting of both inter-layer and intra-layer pipelining. Since all layer weights are hardwired onto the metal layers, the wiring

weights for each layer have their own corresponding computing resources. HNs of each layer can operate simultaneously, which facilitates the straightforward formation of a pipeline between the model layers. Within a layer, we partition the computation into a six-stage pipeline, as shown in Figure 8. Consequently, HNLPU can process up to $6 \times$ layer number of batches simultaneously at peak. For the 36-layers LLM, the maximum batch size can theoretically reach 216.

HNLPU employs the batching strategy similar to the continuous batching [53]. During the **prefill** phase, there are no dependencies between the input tokens of a sequence. This independence allows for massively parallel processing, with tokens flowing through the pipeline stage-by-stage. Consequently, HNLPU can process up to 216 tokens concurrently during prefill. Conversely, the **decode** phase is auto-regressive, meaning the generation of each new token is dependent on the completion of the previous one. However, since different sequences are independent, HNLPU can still process up to 216 sequences simultaneously. In summary, HNLPU supports a maximum batch size of 216 sequences. By leveraging continuous batching, the system dynamically schedules new sequences into the batch as soon as slots are freed by completed ones, thereby ensuring high throughput.

6 Methodology

This section details the methodology used to evaluate proposed HNLPU architecture. We describe our hardware evaluation flow, the system-level modeling for multi-chip design, the model used for performance assessment, and the configurations of all baseline systems.

6.1 Hardware and System-Level Evaluation

Hardware Implementation. We implemented the core components of HNLPU architecture, including HN Array, Control Unit, VEX, Interconnection Engine and on-chip Attention Buffer in RTL with Verilog, and verify the correctness of the RTL design through extensive test cases. We followed a standard ASIC design flow to obtain physical characteristics. The design was synthesized using Synopsys Design Compiler and placed-and-routed using Synopsys IC Compiler, on 5 nm technology. Power consumption was analyzed by PrimeTime PX using workload-derived switching activity (SAIF file) to accurately model both static and dynamic power. On-chip SRAMs were generated and analyzed using Memory Compiler on the same technology node.

Multi-chip System Modeling. Our proposed HNLPU is a 4×4 multi-chip system interconnected via the CXL 3.0 protocol. We evaluated the inter-chip communication latency and power using CNSim [16], a state-of-the-art open-source analysis framework for multi-chip systems. This framework allows for detailed modeling of the network on package topology, accounting for physical layer (PHY) latency, protocol overhead, and physical routing delays in our design. We also built a cycle-level simulator for single-chip performance evaluation.

6.2 Model

We selected the OpenAI GPT-oss 120 B model for system-level evaluation. It is a state-of-the-art open-source MoE large language model built on Llama-style architecture. We used 4-bit quantized version of the model and hardwiring the weights in HN Array. The HNLPU implementation of the model follows partitioning method, dataflow and mapping strategies detailed in Section 4 and Section 5.

6.3 Baseline Configurations

We conducted two sets of experiments to comprehensively evaluate our architecture against relevant baselines.

Embedding Methodology Comparison. This benchmark compares the performance of a single matrix-vector multiplication: 1×1024 input vector with a 1024×128 FP4 weight matrix (typical dimension in an LLM attention block) under various embedding methodologies. We compare three designs at 5 nm technology: **MAC Array (MA)**, a 64 KB SRAM companioned with a conventional computing array of 1024 MACs, **Cell-Embedding (CE)** and **Metal-Embedding (ME)** as illustrated in Figure 3. Regarding area, we compare CE and ME with the 64 KB SRAM only, excluding the arbitrarily-sized computing array.

System-Level Performance Comparison. This experiment compares our full HNLPU architecture against leading commercial systems running the same GPT-oss 120 B model with a 2K token length, with hyperparameters for each system individually tuned to achieve its optimal throughput.

- (1) **NVIDIA H100:** We conducted direct measurements on a server equipped with H100 (80 GB memory, 3.35 TB/s bandwidth) GPU. The model was deployed via TensorRT-LLM, and the reported figures are averaged over multiple runs.
- (2) **Cerebras WSE-3:** The throughput was empirically measured through publicly accessible Cerebras cloud service [1] running the GPT-oss 120 B model. As power measurement on cloud is not practical, we adopted the system power figures reported in [27] instead.
- (3) **HNLPU:** The full system modeled as previous described.

7 Evaluation

7.1 Layout Characteristics

Table 1 presents the area and power breakdown of a single chip in the HNLPU. The HN Array and the Attention Buffer are the dominant components in terms of both area and power. The chip occupies a total area of 827.08 mm^2 and has a power consumption of 308.39 W.

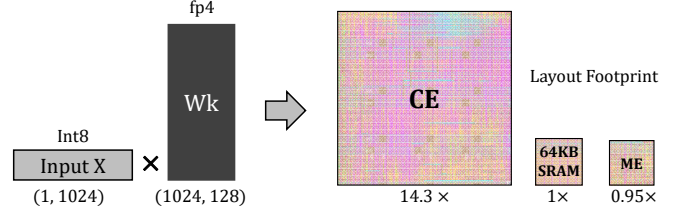


Fig. 9. Area Comparison.



Fig. 10. Time and Energy Comparison.

Table 1. Single Chip Hardware Characteristics

	Area (mm^2)	%	Power (W)	%
HN Array	573.16	69.3	76.92	24.94
VEX	27.87	3.4	33.09	10.73
Control Unit	0.02	0.0	<0.01	0.0
Attention Buffer	136.11	16.5	85.73	27.80
Interconnect Engine	37.92	4.6	49.65	16.10
HBM PHY	52	6.3	63	20.43
Total	827.08	100.0	308.39	100.0

The power density of the HN array is significantly lower than other components due to the sparse circuit activity induced by MoE. Specifically, only 4 out of 128 experts are activated at a time.

7.2 Embedding Methodology Comparison

Figure 9 presents the post-layout area comparison using the SRAM in MA as a base unit. The area of CE/SRAM(MA)/ME is $14.3 \times / 1 \times / 0.95 \times$, respectively, validating the claimed density advantage of ME.

The performance and energy consumption results are illustrated in Figure 10. Both the ME and CE designs demonstrate a dramatic reduction in execution cycles compared to the MA by fully parallelizing the computation. The MA, constrained by the need to fetch weights from SRAM and its limited multiplier array, requires significantly more cycles to complete the same task. The energy reduction of ME is also significant. It consumes the least energy by completely eliminating memory access. While the CE also eliminates power from SRAM access, its massive area leads to substantial leakage power, making it less energy-efficient than ME. The energy consumption of MA is mainly driven by repeated, power-intensive accesses to its SRAM.

In summary, the experimental results demonstrate the comprehensive PPA superiority of the ME design at the operator level. This validates the effectiveness of ME as the fundamental building block for LLM accelerators.

7.3 System-Level Performance Comparison

This section provides a comparison of the system-level performance and efficiency of the HNLPU, NVIDIA H100, and Cerebras WSE-3

Table 2. System-Level Performance and Efficiency Comparison for GPT-oss 120 B Inference

Metric	HNLPU	H100	WSE-3 ^a
<i>Core Performance</i>			
Throughput (tokens/s)	249,960	45	2,940
<i>Physical Characteristics</i>			
Technology Node	5 nm	5 nm	5 nm
Total Silicon Area (mm ²)	13,232	814	46,225
System Footprint (Rack Units)	4 U	1 U	16 U
<i>Power & Efficiency</i>			
Total System Power (kW)	6.9	1.3	23.0
Energy Efficiency (tokens/kJ)	36,226	34.6	127.8
Area Efficiency (tokens/(s·mm²))	18.89	0.055	0.064

^a WSE-3 data is obtained from published reports [2, 27, 38, 50] and calibrated against performance on its public cloud service [1].

on GPT-oss 120 B model, as detailed in Table 2. The HNLPU demonstrates orders-of-magnitude advantages in both throughput and energy efficiency, achieving up to 5,555× and 85× throughput, and 1047× and 283× energy efficiency, respectively. The HNLPU’s superior performance and efficiency stem from a fundamental architectural redesign that diverges from conventional systems.

First, HNLPU physically hardwires model weights into the compute fabric. This creates massive, fine-grained parallelism and inherently supports ultra-high throughput inference.

Second, as a direct consequence, this design completely eliminates the need to access weights from the memory hierarchy (e.g., SRAM, DRAM), thus avoiding the immense energy cost of memory access.

Finally, the HNLPU operates on a highly optimized, model-specific dataflow, workload partitioning, and pipelining strategy, which contrasts with the instruction-driven paradigm of GPUs. This eliminates the significant overhead from control unit such as instruction decoding, scheduling, and control flow. It ensures that nearly all time, power, and area are dedicated to effective computation.

7.4 Economy and Carbon Footprint

To evaluate the economic feasibility of the HNLPU in real-world deployments, this section presents a Total Cost of Ownership (TCO) analysis. We compare a single 32 U rack containing eight HNLPU systems against a commercial cluster of 10,000 NVIDIA H100 GPUs delivering equivalent inference throughput.

For Capital Expenditure (CapEx), the HNLPU’s total CapEx is significantly lower than the total investment required for a 10,000-GPU H100 cluster, despite a substantial Non-Recurring Engineering (NRE) cost of \$184 M.

In terms of Operational Expenditure (OpEx), HNLPU’s total electricity cost over three years is only \$0.19 M. This represents an energy cost reduction of over \$45 M compared to the GPU cluster, enabling green and sustainable AI computation.

Overall, within a three-year lifecycle, the HNLPU’s TCO is nearly 65% lower than that of the GPU cluster. Our analysis explicitly accounts for model updating by including the cost of metal-embedding re-spins. In the demanding scenario of yearly model updates, the HNLPU’s TCO maintains a significant advantage.

We also employ the performance-cost efficiency metric, tokens/(s·\$), to further analyze its economic benefits. The HNLPU achieves 12.65× and 8.57× higher efficiency in the static and yearly-update model scenarios, respectively.

Finally, we estimated the 3-year equivalent carbon dioxide emissions. The HNLPU’s carbon emissions are 780 tons of CO₂e, a figure approximately 234× lower than that of the H100 cluster. Even when considering yearly model updates, its emissions remain 230× lower.

8 Discussion

In Section 7.4, we assume the fabrication of only a single HNLPU, as a single unit is already sufficient to meet the demands of today’s high-volume LLM inference services. We anticipate that the unprecedented performance of HNLPU will unlock novel LLM application scenarios that were impossible otherwise, thereby stimulating further growth in inference volume. If multiple systems are produced, NRE will be further amortized, amplifying the cost advantages.

We estimate the initial NRE cost on making HNLPU chips for various LLMs other than GPT-oss in Table 4. Results suggest that a wide range of model sizes can be deployed within an acceptable budget.

Future works extending HNLPU include: (1) **Design for Process Variation Tolerance (PVT)**, adding hardware redundancy and on-line integrity self-correcting such as Error-Correction Codes (ECC) for higher yield; (2) **Enhanced Flexibility on Sea-of-Neurons**, enabling hyper-parameter updates with annual re-spin by programmable dataflow; (3) **Automated Design and Test**, including an automated Hardwired-Neuron Compiler for shorten delay in the design flow; (4) **Extended Application Scenarios**, implementing LoRA (leaving a small portion of dynamic weights), conditional decoding (programmable sampling algorithms), and support of use cases other than generation (sequence scoring, text-embedding, etc.). (5) **Scalability for Extremely Large Models**, However, we see no obvious technical obstacles towards implementing these features on HNLPU.

9 Related Works

This work is mostly inspired by the current progresses in large language models. The success of GPT-3 has proven that LLMs are few-shot learners [7]. DeepSeek-V3 [55] proved the great benefits from specialization focusing on a single LLM. However, as a software company they have to build upon existing hardware in the market. The *mortal computing* argument from Hinton [23] also partly parallels our vision on extremely specialized LPUs.

The first principle of DNN acceleration has been time-multiplexing hardware neurons and capturing data reuse, a wide belief since DianNao in 2014 [9]. However, the data reuse chances are evaporating from modern LLM inference, which only has ~1 operational intensity in the autoregressive decoding process. Most researchers agree that external memory accesses are the key challenge, while having divergent vision of future. Previous efforts focus on scheduling [8, 11, 37, 43, 44, 53], quantization [13, 17, 28, 34, 41], sparsity [18, 49, 51, 56], speculative decoding [26], and revisiting spiking neurons [26], but these techniques cannot fundamentally

Table 3. Total Cost of Ownership (TCO) Analysis for Large-Scale LLM Inference over a 3-Year Lifecycle

Parameter Category	Single HNLP Server	10,000-GPU H100 cluster	Remarks / Calculation Basis
<i>System Configuration & Power</i>			
Equivalent Throughput	4.44×	1×	Relative performance baseline.
IT Power Load (MW)	0.0552	13	H100: 10k GPUs × 1.3kW.
Total Datacenter Power (MW)	0.0773	18.2	Power Usage Effectiveness (PUE) = 1.4.
<i>Capital Expenditure (CapEx)</i>			
Chips NRE / GPU Price	\$ 184 M	\$ 300 M	Photomasks = \$ 64.6 M, Wafer, Test, Packaging, IP, Tools, Services = \$ 119.4 M
Server / Networking Cost	\$ 2 M	\$ 150 M	Estimated as 50% of GPU price.
Datacenter Infra. Cost	\$ 0.04 M	\$ 35 M	
Total Initial CapEx	\$ 186 M	\$ 485 M	Sum of all CapEx components above.
Annual Update Re-spin Cost	\$ 44.3 M	0	Photomasks = \$ 36.9 M, Wafer, Test, Packaging = \$ 7.4 M
<i>3-Year Operational Expenditure (OpEx)</i>			
Electricity Cost (@ \$0.095/kWh)	\$0.19M	\$45.44M	Total Power × 3 years × \$0.095/kWh [36].
<i>3-Year Total Cost of Ownership (TCO)</i>			
Static Model (No Updates)	\$ 186.2 M	\$ 530.4 M	Total CapEx + 3-Year OpEx.
Dynamic Model (Annual Updates)	\$ 274.8 M	\$ 530.4 M	Static TCO + 2× Update Re-spin.
<i>Performance-Cost Efficiency (Relative)</i>			
Throughput / CapEx	11.58×	1.0×	Relative Throughput / Total Initial CapEx.
Throughput / TCO (Static)	12.65×	1.0×	Relative Throughput / Static TCO.
Throughput / TCO (Dynamic)	8.57×	1.0×	Relative Throughput / Dynamic TCO.
<i>Sustainable AI Support</i>			
Total tCO ₂ e Emissions (Static / Dynamic)	780 / 794	182,321	Following [20, 30, 57], including embodied and operational emissions.

Table 4. Chip NRE prices on various models.

	Kimi-K2 [46]	DeepSeek-V3 [32]	QwQ [42]	Llama-3 [15]
Param. #	1 T	671 B	32 B	8 B
Price/M\$	462	353	69	38

solve the memory access issue. The Process-In-Memory (PIM) architecture has attracted considerable attention owing to its ability to reduce data movement and alleviate external memory accesses [19, 21, 22, 33, 54]. However, it cannot fundamentally eliminate the memory accesses required for weight loading, or suffer from high AD/DA overhead.

After the success of LLM, Language Processing Units (LPU) are emerging as the next important processor scheme. Groq released the first commercialized LPU, rebranded from its Tensor Streaming Multiprocessor in 2022 [4], which attempts to address the issue by incorporating huge on-chip SRAM. Etched Sohu [3] is the most aggressively specialized LPU project that etched Transformer model architecture directly in the fabric. However, these LPUs failed to etch weights, possibly due to the density and cost limitation explained in Section 2. Proposed by this paper, we expect that Metal-Embedding will be the prerequisite technology for the emerging fully-specialized LPU products.

Metal-Embedding shares some underlying techniques with existing architectures: Primitivization architecture proposed by Cambricon-C [10], bit-serial architecture explored by Stripes [24], and the prefabricated wafers once emerged as sea-of-gates architecture in 1990s [14].

10 Conclusions

This paper introduces the Hardwired-Neurons Language Processing Unit (HNLP), an extremely specialized processor that hardwires LLM weight parameters into its compute fabric. Enabled by a novel Metal-Embedding methodology that encodes weights in the 3D topology of metal wires, the design achieves a 15× density improvement and reduces photomask costs by 112×. The resulting system demonstrates unprecedented efficiency, delivering a 5,555× throughput gain and a 1,047× energy efficiency improvement over H100, establishing an economically viable, sustainable, ultra-high-performance cognitive substrate for general tasks.

References

- [1] 2024. Cerebras Inference. <https://www.cerebras.ai/inference>
- [2] 2024. Cerebras System. <https://www.cerebras.ai/system>
- [3] 2025. Etched.ai – Sohu (transformer ASIC). <https://en.wikipedia.org/wiki/Etched.ai>. Accessed: 2025-08-19.
- [4] Dennis Abts, Garrin Kimmell, Andrew Ling, John Kim, Matt Boyd, Andrew Bitar, Sahil Parmar, Ibrahim Ahmed, Roberto DiCecco, David Han, et al. 2022. A software-defined tensor streaming multiprocessor for large-scale machine learning. In *Proceedings of the 49th Annual International Symposium on Computer Architecture*. 567–580.
- [5] Dennis Abts, Jonathan Ross, Jonathan Sparling, Mark Wong-VanHaren, Max Baker, Tom Hawkins, Andrew Bell, John Thompson, Temesghen Kahsai, Garrin Kimmell, et al. 2020. Think fast: A tensor streaming processor (TSP) for accelerating deep learning workloads. In *2020 ACM/IEEE 47th Annual International Symposium on Computer Architecture (ISCA)*. IEEE, 145–158.
- [6] Reza Yazdani Aminabadi, Samyam Rajbhandari, Ammar Ahmad Awan, Cheng Li, Du Li, Elton Zheng, Olatunji Ruwase, Shaden Smith, Minjia Zhang, Jeff Rasley, et al. 2022. Deepspeed-inference: enabling efficient inference of transformer models at unprecedented scale. In *SC22: International Conference for High Performance Computing, Networking, Storage and Analysis*. IEEE, 1–15.
- [7] Tom Brown, Benjamin Mann, Nick Ryder, Melanie Subbiah, Jared D Kaplan, Prafulla Dhariwal, Arvind Neelakantan, Pranav Shyam, Girish Sastry, Amanda Askell, et al. 2020. Language models are few-shot learners. *Advances in neural information processing systems* 33 (2020), 1877–1901.
- [8] Jingwei Cai, Xuan Wang, Mingyu Gao, Sen Peng, Zijian Zhu, Yuchen Wei, Zuotong Wu, and Kaisheng Ma. 2025. Soma: Identifying, exploring, and understanding

- the dram communication scheduling space for dnn accelerators. In *2025 IEEE International Symposium on High Performance Computer Architecture (HPCA)*. IEEE, 533–548.
- [9] Tianshi Chen, Zidong Du, Ninghui Sun, Jia Wang, Chengyong Wu, Yunji Chen, and Olivier Temam. 2014. Diannao: A small-footprint high-throughput accelerator for ubiquitous machine-learning. *ACM SIGARCH Computer Architecture News* 42, 1 (2014), 269–284.
- [10] Yi Chen, Yongwei Zhao, Yifan Hao, Yuanbo Wen, Yuntao Dai, Xiaqing Li, Yang Liu, Rui Zhang, Mo Zou, Xinkai Song, Xing Hu, Zidong Du, Huaping Chen, Qi Guo, and Tianshi Chen. 2024. Cambricon-C: Efficient 4-Bit Matrix Unit via Primitivization. In *Proceedings of the 2024 57th IEEE/ACM International Symposium on Microarchitecture* (Austin, TX, USA) (MICRO '24). IEEE Press, 538–550. doi:10.1109/MICRO61859.2024.00047
- [11] Shenggan Cheng, Shengjie Lin, Lansong Diao, Hao Wu, Siyu Wang, Chang Si, Ziming Liu, Xuanlei Zhao, Jianguo Du, Wei Lin, et al. 2025. Concerto: Automatic Communication Optimization and Scheduling for Large-Scale Deep Learning. In *Proceedings of the 30th ACM International Conference on Architectural Support for Programming Languages and Operating Systems, Volume 1*. 198–213.
- [12] Common Crawl. [n. d.]. Overview | Common Crawl. <https://commoncrawl.org/overview> Accessed: 2025-08-19.
- [13] Bitar Darvish Rouhani, Ritchie Zhao, Venmugil Elango, Rasoul Shafipour, Mathew Hall, Maral Mesmakhoshahi, Ankit More, Levi Melnick, Maximilian Golub, Girish Varatkar, et al. 2023. With shared microexponents, a little shifting goes a long way. In *Proceedings of the 50th Annual International Symposium on Computer Architecture*. 1–13.
- [14] Manoel E. de Lima and David J. Kinniment. 1995. Sea-of-gates architecture. *Microelectronics Journal* 26, 5 (1995), 431–440. doi:10.1016/0026-2692(95)98945-N
- [15] Abhimanyu Dubey, Abhinav Jauhri, Abhinav Pandey, Abhishek Kadian, Ahmad Al-Dahle, Aiesha Letman, Akhil Mathur, Alan Schelten, Amy Yang, Angela Fan, et al. 2024. The llama 3 herd of models. *arXiv e-prints* (2024), arXiv–2407.
- [16] Yinxiao Feng, Yuchen Wei, Dong Xiang, and Kaisheng Ma. 2024. Evaluating chiplet-based large-scale interconnection networks via cycle-accurate packet-parallel simulation. In *Proceedings of the 2024 USENIX Conference on Usenix Annual Technical Conference (USENIX ATC'24)*. USENIX Association, Article 45, 17 pages.
- [17] Minseong Gil, Dongho Ha, Simla Burcu Harma, Myung Kuk Yoon, Babak Falsafi, Won Woo Ro, and Yunho Oh. 2025. Avant-Garde: Empowering GPUs with Scaled Numeric Formats. In *Proceedings of the 52nd Annual International Symposium on Computer Architecture*. 153–165.
- [18] Ashish Gondimalla, Mithuna Thottethodi, and TN Vijaykumar. 2023. Eureka: Efficient tensor cores for one-sided unstructured sparsity in dnn inference. In *Proceedings of the 56th Annual IEEE/ACM International Symposium on Microarchitecture*. 324–337.
- [19] Yufeng Gu, Alireza Khadem, Sumanth Umesh, Ning Liang, Xavier Servot, Onur Mutlu, Ravi Iyer, and Reetuparna Das. 2025. PIM is all you need: A CXL-enabled GPU-free system for large language model inference. In *Proceedings of the 30th ACM International Conference on Architectural Support for Programming Languages and Operating Systems, Volume 2*. 862–881.
- [20] Udit Gupta, Mariam Elgamal, Gage Hills, Gu-Yeon Wei, Hsien-Hsin S Lee, David Brooks, and Carole-Jean Wu. 2022. ACT: designing sustainable computer systems with an architectural carbon modeling tool. In *Proceedings of the 49th Annual International Symposium on Computer Architecture*. 784–799.
- [21] Yintao He, Haiyu Mao, Christina Giannoula, Mohammad Sadrosadati, Juan Gómez-Luna, Huawei Li, Xiaowei Li, Ying Wang, and Onur Mutlu. 2025. PAPI: Exploiting Dynamic Parallelism in Large Language Model Decoding with a Processing-In-Memory-Enabled Computing System. In *Proceedings of the 30th ACM International Conference on Architectural Support for Programming Languages and Operating Systems, Volume 2* (Rotterdam, Netherlands) (ASPLOS '25). Association for Computing Machinery, New York, NY, USA, 766–782. doi:10.1145/3676641.3716009
- [22] Guseul Heo, Sangyeop Lee, Jaehong Cho, Hyunmin Choi, Sanghyeon Lee, Hyungkyu Ham, Gwangsun Kim, Divya Mahajan, and Jongse Park. 2024. Neupims: Npu-pim heterogeneous acceleration for batched llm inferring. In *Proceedings of the 29th ACM International Conference on Architectural Support for Programming Languages and Operating Systems, Volume 3*. 722–737.
- [23] Geoffrey Hinton. 2023. Two Paths to Intelligence. *Public Lecture, University of Cambridge* (2023).
- [24] Patrick Judd, Jorge Albericio, Tayler Hetherington, Tor M. Aamodt, and Andreas Moshovos. 2016. Stripes: Bit-serial deep neural network computing. In *2016 49th Annual IEEE/ACM International Symposium on Microarchitecture (MICRO)*. 1–12. doi:10.1109/MICRO.2016.7783722
- [25] Paul HJ Kelly. 2020. "Turing Tariff" reduction: Architectures, compilers and languages to break the universality barrier.
- [26] Sangyeob Kim, Sangjin Kim, Wooyoung Jo, Soyeon Kim, Seongyun Hong, and Hoi-Jun Yoo. 2024. 20.5 C-Transformer: A 2.6-18.1uJ/Token Homogeneous DNN-Transformer/Spiking-Transformer Processor with Big-Little Network and Implicit Weight Generation for Large Language Models. In *2024 IEEE International Solid-State Circuits Conference (ISSCC)*, Vol. 67. 368–370. doi:10.1109/ISSCC49657.2024.10454330
- [27] Yudhishthira Kundu, Manroop Kaur, Tripty Wig, Kriti Kumar, Pushpanjali Kumari, Vivek Puri, and Manish Arora. 2025. A Comparison of the Cerebras Wafer-Scale Integration Technology with Nvidia GPU-based Systems for Artificial Intelligence. arXiv:2503.11698 [cs.AR]
- [28] Alberto Delmas Lascorz, Mostafa Mahmoud, Ali Hadi Zadeh, Milos Nikolic, Kareem Ibrahim, Christina Giannoula, Ameer Abdelhadi, and Andreas Moshovos. 2024. Atalanta: A bit is worth a "thousand" tensor values. In *Proceedings of the 29th ACM International Conference on Architectural Support for Programming Languages and Operating Systems, Volume 2*. 85–102.
- [29] Gary Lauterbach. 2021. The path to successful wafer-scale integration: The cerebras story. *IEEE Micro* 41, 6 (2021), 52–57.
- [30] Yueying Li, Zhanqiu Hu, Esha Choukse, Rodrigo Fonseca, G Edward Suh, and Udit Gupta. 2025. Ecoserve: Designing carbon-aware ai inference systems. *arXiv preprint arXiv:2502.05043* (2025).
- [31] Sean Lie. 2023. Cerebras architecture deep dive: First look inside the hardware/software co-design for deep learning. *IEEE Micro* 43, 3 (2023), 18–30.
- [32] Aixin Liu, Bei Feng, Bing Xue, Bingxuan Wang, Bochao Wu, Chengda Lu, Chenggang Zhao, Chengqi Deng, Chenyu Zhang, Chong Ruan, et al. 2024. Deepseek-v3 technical report. *arXiv preprint arXiv:2412.19437* (2024).
- [33] Jiantao Liu, Minxuan Zhou, Yue Pan, Chien-Yi Yang, Lana Josipović, and Tajana Rosing. 2025. OptiPIM: Optimizing Processing-in-Memory Acceleration Using Integer Linear Programming. In *Proceedings of the 52nd Annual International Symposium on Computer Architecture*. 867–883.
- [34] Zihan Liu, Xinhao Luo, Junxian Guo, Wentao Ni, Yangjie Zhou, Yue Guan, Cong Guo, Weihao Cui, Yu Feng, Minyi Guo, et al. 2025. VQ-LLM: High-performance Code Generation for Vector Quantization Augmented LLM Inference. In *2025 IEEE International Symposium on High Performance Computer Architecture (HPCA)*. IEEE, 1496–1509.
- [35] Gary Luyyan and Andy Clark. 2015. Words and the world: Predictive coding and the language-perception-cognition interface. *Current Directions in Psychological Science* 24, 4 (2015), 279–284.
- [36] Massed Compute. 2024. What are the average electricity costs for data centers in different regions and how do they impact total costs? <https://massedcompute.com/faq-answers/?question=What+are+the+average+electricity+costs+for+data+centers+in+different+regions+and+how+do+they+impact+total+costs%3F>. Accessed: 2025-08-20.
- [37] Yixuan Mei, Yonghao Zhuang, Xupeng Miao, Juncheng Yang, Zhihao Jia, and Rashmi Vinayak. 2025. Helix: Serving large language models over heterogeneous gpus and network via max-flow. In *Proceedings of the 30th ACM International Conference on Architectural Support for Programming Languages and Operating Systems, Volume 1*. 586–602.
- [38] Sebastian Moss. 2025. Cerebras unveils four trillion-transistor giant chip. <https://www.datacenterdynamics.com/en/news/cerebras-unveils-four-trillion-transistor-giant-chip-targets-generative-ai/>
- [39] US Department of Energy. 2024. DOE Releases New Report Evaluating Increase in Electricity Demand from Data Centers. (2024). <https://www.energy.gov/articles/doe-releases-new-report-evaluating-increase-electricity-demand-data-centers>
- [40] OpenAI. 2025. Introducing GPT-OSS. <https://openai.com/index/introducing-gpt-oss/>. Accessed: 2025-08-19.
- [41] Yubin Qin, Yang Wang, Jiachen Wang, Zhiwei Lin, Yushu Zhao, Shaojun Wei, Yang Hu, and Shouyi Yin. 2025. 23.8 An 88.36TOPS/W Bit-Level-Weight-Compressed Large-Language-Model Accelerator with Cluster-Aligned INT-FP-GEMM and Bi-Dimensional Workflow Reformulation. In *2025 IEEE International Solid-State Circuits Conference (ISSCC)*, Vol. 68. 420–422. doi:10.1109/ISSCC49661.2025.10904774
- [42] Qwen. 2025. QwQ-32B: Embracing the Power of Reinforcement Learning. <https://qwenlm.github.io/blog/qwq-32b/>. Blog post.
- [43] Karthikeyan Sankaralingam, Tony Nowatzki, Vinay Gangadhar, Preyas Shah, Michael Davies, William Galliher, Ziliang Guo, Jitu Khare, Deepak Vijay, Poly Palamuttam, et al. 2022. The Mozart reuse exposed dataflow processor for AI and beyond: Industrial product. In *Proceedings of the 49th Annual International Symposium on Computer Architecture*. 978–992.
- [44] Jovan Stojkovic, Chaojie Zhang, Inigo Goiri, Esha Choukse, Haoran Qiu, Rodrigo Fonseca, Josep Torrellas, and Ricardo Bianchini. 2025. Tapas: Thermal-and power-aware scheduling for LLM inference in cloud platforms. In *Proceedings of the 30th ACM International Conference on Architectural Support for Programming Languages and Operating Systems, Volume 2*. 1266–1281.
- [45] Vivienne Sze, Yu-Hsin Chen, Tien-Ju Yang, and Joel S Emer. 2017. Efficient processing of deep neural networks: A tutorial and survey. *Proc. IEEE* 105, 12 (2017), 2295–2329.
- [46] Kimi Team, Yifan Bai, Yiping Bao, Guanduo Chen, Jiahao Chen, Ningxin Chen, Ruijue Chen, Yanru Chen, Yuankun Chen, Yutian Chen, et al. 2025. Kimi k2: Open agentic intelligence. *arXiv preprint arXiv:2507.20534* (2025).
- [47] Ashish Vaswani, Noam Shazeer, Niki Parmar, Jakob Uszkoreit, Llion Jones,

- Aidan N Gomez, Lukasz Kaiser, and Illia Polosukhin. 2017. Attention is all you need. *Advances in neural information processing systems* 30 (2017).
- [48] Bin Wang, Bojun Wang, Changyi Wan, Guanzhe Huang, Hanpeng Hu, Haonan Jia, Hao Nie, Mingliang Li, Nuo Chen, Siyu Chen, et al. 2025. Step-3 is Large yet Affordable: Model-system Co-design for Cost-effective Decoding. *arXiv preprint arXiv:2507.19427* (2025).
- [49] Huizheng Wang, Jiahao Fang, Xinru Tang, Zhiheng Yue, Jinxi Li, Yubin Qin, Sihan Guan, Qinze Yang, Yang Wang, Chao Li, et al. 2024. SOFA: A compute-memory optimized sparsity accelerator via cross-stage coordinated tiling. In *2024 57th IEEE/ACM International Symposium on Microarchitecture (MICRO)*. IEEE, 1247–1263.
- [50] James Wang. 2024. Cerebras CS-3: the world’s fastest and most scalable AI accelerator. <https://www.cerebras.ai/blog/cerebras-cs3>
- [51] Yang Wang, Yubin Qin, Dazheng Deng, Jingchuan Wei, Yang Zhou, Yuanqi Fan, Tianbao Chen, Hao Sun, Leibo Liu, Shaojun Wei, et al. 2022. A 28nm 27.5 TOPS/W approximate-computing-based transformer processor with asymptotic sparsity speculating and out-of-order computing. In *2022 IEEE international solid-state circuits conference (ISSCC)*, Vol. 65. IEEE, 1–3.
- [52] Jason Wei, Yi Tay, Rishi Bommasani, Colin Raffel, Barret Zoph, Sebastian Borgeaud, Dani Yogatama, Maarten Bosma, Denny Zhou, Donald Metzler, et al. 2022. Emergent abilities of large language models. *arXiv preprint arXiv:2206.07682* (2022).
- [53] Gyeong-In Yu, Joo Seong Jeong, Geon-Woo Kim, Soojeong Kim, and Byung-Gon Chun. 2022. Orca: A distributed serving system for {Transformer-Based} generative models. In *16th USENIX Symposium on Operating Systems Design and Implementation (OSDI 22)*. 521–538.
- [54] Zhiheng Yue, Xujiang Xiang, Yang Wang, Ruiqi Guo, Huiming Han, Shaojun Wei, Yang Hu, and Shouyi Yin. 2025. 14.4 A 51.6TFLOPs/W Full-Datapath CIM Macro Approaching Sparsity Bound and <2-30 Loss for Compound AI. In *2025 IEEE International Solid-State Circuits Conference (ISSCC)*, Vol. 68. 1–3. doi:10.1109/ISSCC49661.2025.10904702
- [55] Chenggang Zhao, Chengqi Deng, Chong Ruan, Damai Dai, Huazuo Gao, Jiashi Li, Liyue Zhang, Panpan Huang, Shangyan Zhou, Shirong Ma, Wenfeng Liang, Ying He, Yuqing Wang, Yuxuan Liu, and Y.X. Wei. 2025. Insights into DeepSeek-V3: Scaling Challenges and Reflections on Hardware for AI Architectures. In *Proceedings of the 52nd Annual International Symposium on Computer Architecture (ISCA '25)*. Association for Computing Machinery, New York, NY, USA, 1731–1745. doi:10.1145/3695053.3731412
- [56] Youpeng Zhao, Di Wu, and Jun Wang. 2024. Alisa: Accelerating large language model inference via sparsity-aware kv caching. In *2024 ACM/IEEE 51st Annual International Symposium on Computer Architecture (ISCA)*. IEEE, 1005–1017.
- [57] Yujie Zhao, Yang Zhao, Cheng Wan, and Yingyan Lin. 2024. 3d-carbon: An analytical carbon modeling tool for 3d and 2.5 d integrated circuits. In *Proceedings of the 61st ACM/IEEE Design Automation Conference*. 1–6.